Dispersion Reduction of a Direct-Fire Rocket Using Lateral Pulse Jets

by Thanat Jitpraphai and Mark Costello

ARL-CR-465 April 2001

prepared by

Thanat Jitpraphai and Mark Costello
Oregon State University
Corvallis, Oregon 97331

under contract

DAAD17-00-P-0853

Army Research Laboratory
Aberdeen Proving Ground, MD 21005-5066

ARL-CR-465 **April 2001**

Dispersion Reduction of a Direct-Fire Rocket Using Lateral Pulse Jets

Thanat Jitpraphai and Mark Costello
Oregon State University

Abstract

The impact point dispersion of a direct-fire rocket can be drastically reduced with a ring of appropriately sized lateral pulse jets coupled to a trajectory tracking flight control system. The system is shown to work well against uncertainty in the form of initial off-axis angular velocity perturbations as well as atmospheric winds. In an example case, dispersion was reduced by a factor of 100. Dispersion reduction is a strong function of the number of individual pulse jets, the pulse jet impulse, and the trajectory tracking window size. Properly selecting these parameters for a particular rocket and launcher combination is required to achieve optimum dispersion reduction. For relatively low pulse jet impulse, dispersion steadily decreases as the number of pulse jets is increased or as the pulse jet impulse is increased. For a fixed total pulse jet ring impulse, a single pulse is the optimum pulse jet configuration when the pulse jet ring impulse is small due to the fact that the effect of a pulse on the trajectory of a rocket decreases as the round flies down range.

Contents

INTENTIONALLY LEFT BLANK.

List of Figures

INTENTIONALLY LEFT BLANK.

1. Introduction

Uncontrolled direct fire rockets exhibit high impact point dispersion, even at relatively short range, and as such have been employed as area weapons on the battlefield. Because direct fire rockets exit the launcher with low velocity, any aerodynamic disturbances presented to the rocket near the launcher create relatively large angles of attack, leading to large aerodynamic jump and increased target dispersion. Furthermore, main rocket motor thrust during the initial portion of flight tends to amplify the effect of initial transverse and angular velocity perturbations on dispersion. The integrated effect over the trajectory of initial disturbances as the rocket enters atmospheric flight and high sensitivity to atmospheric disturbances all lead to large impact point dispersion.

Increased design requirements being placed on direct fire ammunition, including direct fire rockets, call for surgical removal of select targets on the battlefield. Economic realities now stipulate that improved capability be delivered at reduced unit cost. Small, rugged, and inexpensive microelectromechanical sensors (MEMS) coupled to a suitable and inexpensive control mechanism offer the potential to meet these increasingly stringent design requirements. A potential control mechanism that is small, durable, and can be located in close proximity to the sensor suite is a lateral pulse jet ring mounted forward on the rocket body. The pulse jet ring consists of a finite number of individual pulse jets. Each pulse jet on the ring imparts a single, short duration, large force to the rocket in the plane normal to the rocket axis of symmetry.

Several investigators have explored the loads caused by a lateral pulse jet on a projectile body. Srivastava [1] showed good agreement between computational and experimental results for the normal force and pitching moment of a lateral jet operating on a supersonic missile. Later, Srivastava [2] showed that lateral thrust jet effectiveness diminished as the jet thruster was gradually rolled toward the windward side of the missile. Brandeis and Gill [3] performed an experimental investigation of effect of a lateral jet on the forces and moments on a supersonic missile. They showed that jet force amplification strongly depends on the size and location of lifting surfaces of the missile and that jet force amplification is inversely proportional to jet pressure. Using lateral pulse jets to improve target dispersion performance has been investigated by Harkins and Brown [4]. They used a set of lateral pulse jets to eliminate the off-axis angular rate of the projectile just after exiting the launcher. For the notional concepts considered, dispersion was reduced by a factor of four.

The work reported here seeks to reduce the dispersion of an atmospheric rocket using a trajectory tracking flight control system. Pulse jet firing logic is engaged when the trajectory tracking error exceeds a specific threshold. Parametric trade studies that consider the effect of the number of pulse jets, pulse jet impulse, and trajectory tracking window size on impact point dispersion were conducted.

2. Direct-Fire Rocket Dynamic Model

The numerical simulation employed in this study consists of a rigid body six degree of freedom model typically utilized in flight dynamic modeling of projectiles. A schematic of the direct-fire rocket configuration with major elements of the system identified is given in Figure 1. The degrees of freedom include three position components of the mass center of the rocket as well as three Euler orientation angles of the body. The equations of motion are provided in equations 1–4 [5, 6].

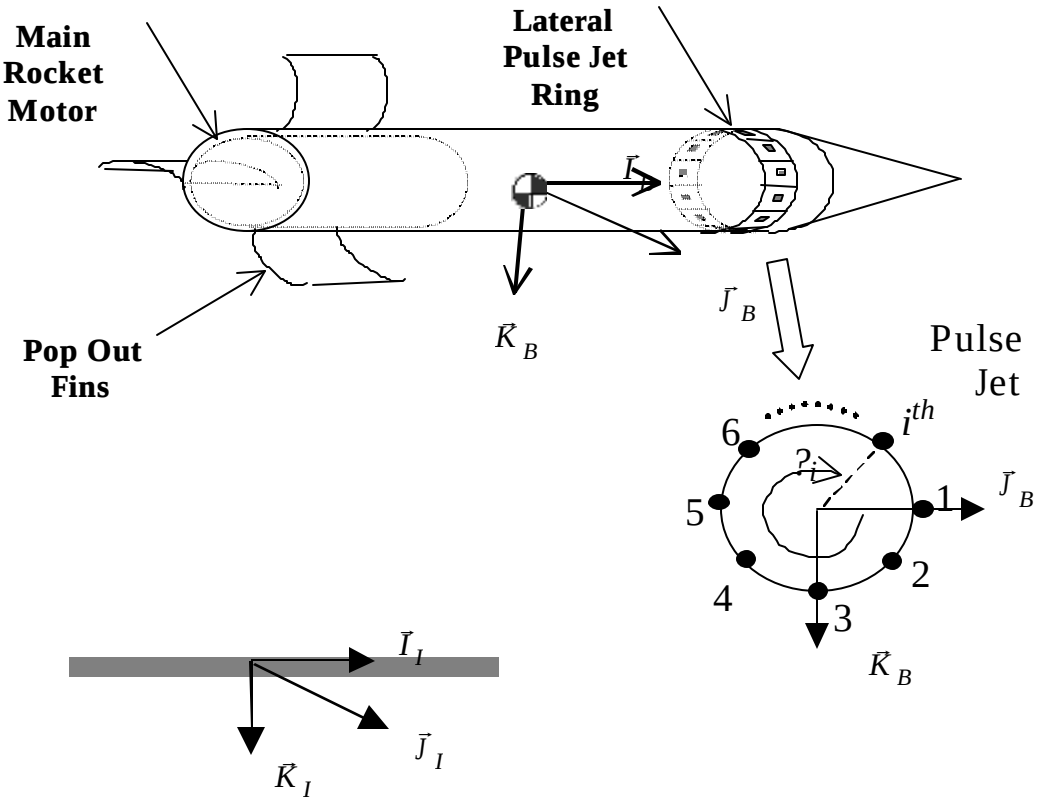

Figure 1. Schematic of a direct-fire rocket with a lateral pulse jets.

$$\begin{Bmatrix}\dot{x}\\ \dot{y}\\ \dot{z}\end{Bmatrix}=\begin{bmatrix}c_? c_? & s_f s_? c_? - c_f s_? & c_f s_? c_? + s_f s_?\\ c_? s_? & s_f s_? s_? + c_f c_? & c_f s_? s_? - s_f c_?\\ -s_? & s_f c_? & c_f c_?\end{bmatrix}\begin{Bmatrix}u\\ v\\ w\end{Bmatrix}. \tag{1}$$

$$\begin{Bmatrix}\dot{\phi}\\ \dot{\theta}\\ \dot{\psi}\end{Bmatrix}=\begin{bmatrix}1 & s_\phi t_\theta & c_\phi t_\theta\\ 0 & c_\phi & -s_\phi\\ 0 & s_\phi / c_\theta & c_\phi / c_\theta\end{bmatrix}\begin{Bmatrix}p\\ q\\ r\end{Bmatrix}. \tag{2}$$

$$\begin{Bmatrix}\dot{u}\\ \dot{v}\\ \dot{w}\end{Bmatrix}=\begin{Bmatrix}X/m\\ Y/m\\ Z/m\end{Bmatrix}-\begin{bmatrix}0 & -r & q\\ r & 0 & -p\\ -q & p & 0\end{bmatrix}\begin{Bmatrix}u\\ v\\ w\end{Bmatrix}. \tag{3}$$

$$\begin{Bmatrix}\dot{p}\\ \dot{q}\\ \dot{r}\end{Bmatrix}=[I]^{-1}\left[\begin{Bmatrix}L\\ M\\ N\end{Bmatrix}-\begin{bmatrix}0 & -r & q\\ r & 0 & -p\\ -q & p & 0\end{bmatrix}[I]\begin{Bmatrix}p\\ q\\ r\end{Bmatrix}\right]. \tag{4}$$

The applied loads appearing in equation 3 contain contributions from rocket weight ($_W$), air loads ($_A$), main rocket thrust ($_R$), and lateral pulse jet forces ($_J$).

$$\begin{Bmatrix}X\\ Y\\ Z\end{Bmatrix}=\begin{Bmatrix}X_W\\ Y_W\\ Z_W\end{Bmatrix}+\begin{Bmatrix}X_A\\ Y_A\\ Z_A\end{Bmatrix}+\begin{Bmatrix}X_R\\ Y_R\\ Z_R\end{Bmatrix}+\begin{Bmatrix}X_J\\ Y_J\\ Z_J\end{Bmatrix}. \tag{5}$$

The rocket weight contribution is given by equation 6,

$$\begin{Bmatrix}X_W\\ Y_W\\ Z_W\end{Bmatrix}=mg\begin{Bmatrix}-s_\theta\\ s_\phi c_\theta\\ c_\phi c_\theta\end{Bmatrix}, \tag{6}$$

while the air loads contribution, which acts at the center of pressure of the rocket, is given by equation 7.

$$\begin{Bmatrix}X_A\\ Y_A\\ Z_A\end{Bmatrix}=-\frac{\pi}{8}\rho V_A^2 D^2\begin{Bmatrix}C_{X0}+C_{X2}(v_A^2+w_A^2)/V_A^2\\ C_{NA}v_A/V_A\\ C_{NA}w_A/V_A\end{Bmatrix}. \tag{7}$$

The main rocket motor increases the velocity of the rocket by providing high thrust levels during the initial portion of the trajectory. In some direct-fire rocket designs, the exhaust nozzle contains several flutes such that the exiting flow is turned, causing (in aggregate) a rolling moment. To account for this effect, the numerical simulation models the main rocket motor as a set of four smaller rocket motors that act as point forces on the body. The position and thrust

orientation of each small rocket motor on the body are determined to match known inertial properties before and after burn and to match a specified roll time trace. Equation 8 provides the main rocket motor force formula.

$$\begin{Bmatrix} X_R \\ Y_R \\ Z_R \end{Bmatrix} = \sum_{i=1}^{4} T_{Ri} \begin{Bmatrix} n_{RXi} \\ n_{RYi} \\ n_{RZi} \end{Bmatrix}. \tag{8}$$

In equation 8, the thrust amplitude profile, T_{R_i}, is a known function of time. The lateral pulse jet forces are modeled in the same manner as the main rocket motor with two exceptions. Since the lateral pulse jets are active over a very short duration of time compared to the time scale of a complete rocket trajectory, the thrust force is modeled as a constant when active. Also, since by definition a lateral pulse jet acts in the $\vec{j}_B$ and $\vec{k}_B$ plane, the $\vec{i}_B$ component of the lateral pulse jet force is zero. Equation 9 provides the lateral pulse jet force formula.

$$\begin{Bmatrix} X_J \\ Y_J \\ Z_J \end{Bmatrix} = \sum_{i=1}^{n_J} T_{Ji} \begin{Bmatrix} 0 \\ -\cos\left(2\pi(i-1)/n_J\right) \\ -\sin\left(2\pi(i-1)/n_J\right) \end{Bmatrix}. \tag{9}$$

The pulse jet ring is located on the skin of the projectile and near the nose of the rocket. Individual pulse jets are uniformly distributed azimuthally around the lateral pulse jet ring. A key feature of the pulse jet configuration considered here is that each pulse jet can be fired only once.

The applied moments about the rocket mass center contains contributions from steady air loads ($_{SA}$), unsteady air loads ($_{UA}$), main rocket thrust ($_R$), and lateral pulse jet forces ($_J$).

$$\begin{Bmatrix} L \\ M \\ N \end{Bmatrix} = \begin{Bmatrix} L_{SA} \\ M_{SA} \\ N_{SA} \end{Bmatrix} + \begin{Bmatrix} L_{UA} \\ M_{UA} \\ N_{UA} \end{Bmatrix} + \begin{Bmatrix} L_R \\ M_R \\ N_R \end{Bmatrix} + \begin{Bmatrix} L_J \\ M_J \\ N_J \end{Bmatrix}. \tag{10}$$

The moment components due to steady aerodynamic forces, main rocket motor forces, and lateral pulse jet forces are computed with a cross product between the distance vector from the mass center of the rocket and the location of the specific force and the force itself. The unsteady body aerodynamic moment provides a damping source for projectile angular motion and is given by equation 11.

$$\begin{Bmatrix} L_{UA} \\ M_{UA} \\ N_{UA} \end{Bmatrix} = \frac{\pi}{8}\rho V_A^2 D^3 \begin{Bmatrix} C_{DD} + \dfrac{pDC_{LP}}{2V_A} \\ \dfrac{qDC_{MQ}}{2V_A} \\ \dfrac{rDC_{MQ}}{2V_A} \end{Bmatrix}. \tag{11}$$

When the rocket motors are active, the mass, mass center location, and inertial properties of the rocket are updated continuously. The center of pressure location and all aerodynamic coefficients depend on local Mach number. The air velocity of the mass center of the rocket includes contributions from inertial motion of the round and atmospheric mean wind. The mean atmospheric wind acts in the horizontal plane and is directed at an angle ψ_{MW} from the $\vec{i}_I$ axis.

$$\begin{Bmatrix} u_A \\ v_A \\ w_A \end{Bmatrix} = \begin{Bmatrix} u \\ v \\ w \end{Bmatrix} + \begin{bmatrix} c_\theta c_\psi & c_\theta s_\psi & -s_\theta \\ s_\phi s_\theta c_\psi - c_\phi s_\psi & s_\phi s_\theta s_\psi + c_\phi c_\psi & s_\phi c_\theta \\ c_\phi s_\theta c_\psi + s_\phi s_\psi & c_\phi s_\theta s_\psi - s_\phi c_\psi & c_\phi c_\theta \end{bmatrix} \begin{Bmatrix} V_{MW} c_{\psi_{MW}} \\ V_{MW} s_{\psi_{MW}} \\ 0 \end{Bmatrix}. \tag{12}$$

As shown in equation 13, the magnitude of the atmospheric mean wind velocity is a function of projectile altitude.

$$V_{MW} = 0.636619\sigma_{MW} \tan^{-1}\left(\frac{z}{1000}\right). \tag{13}$$

In equation 13, s_{MW} is the mean wind intensity.

3. Direct-Fire Rocket Flight Control System

The flight control system seeks to track a prespecified command trajectory utilizing the control authority provided by the lateral pulse jets. A schematic of the flight control system block diagram is shown in Figure 2, while a schematic of the lateral pulse jet firing logic is given in Figure 3. For direct-fire rockets, a command ballistic trajectory is available from the fire control system and can be downloaded to the round just prior to launch. The trajectory tracking flight control system first compares the measured position of the projectile to the commanded trajectory to form a position error vector in the inertial frame. The trajectory error is converted to the rocket body frame using equation 14.

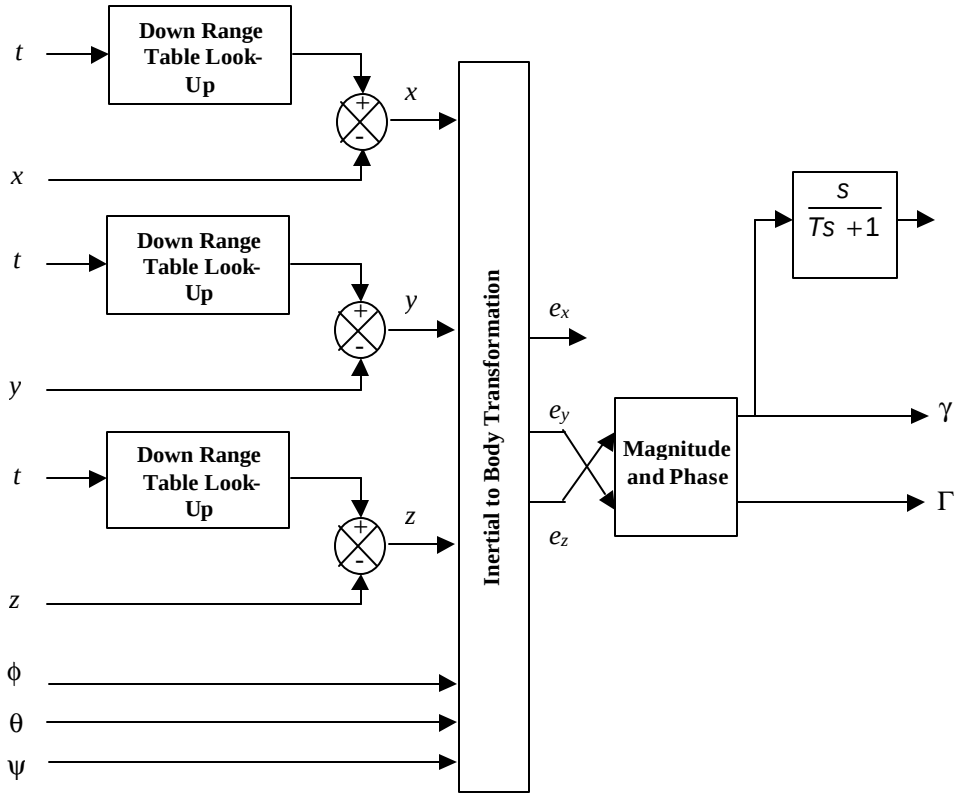

Figure 2. Trajectory tracking flight control system.

$$\begin{Bmatrix} e_X \\ e_Y \\ e_Z \end{Bmatrix} = \begin{bmatrix} c_\theta c_\psi & c_\theta s_\psi & -s_\theta \\ s_\phi s_\theta c_\psi - c_\phi s_\psi & s_\phi s_\theta s_\psi + c_\phi c_\psi & s_\phi c_\theta \\ c_\phi s_\theta c_\psi + s_\phi s_\psi & c_\phi s_\theta s_\psi - s_\phi c_\psi & c_\phi c_\theta \end{bmatrix} \begin{Bmatrix} x_C - x \\ y_C - y \\ z_C - z \end{Bmatrix}. \tag{14}$$

The magnitude and phase of the error in the off-axis plane of the rocket are denoted Γ and γ, and are defined by equations 15 and 16, respectively.

$$\Gamma = \sqrt{e_X^2 + e_Y^2}\,. \tag{15}$$

$$\gamma = \tan^{-1}\left(e_Z / e_Y\right). \tag{16}$$

At each computation cycle in the flight control system, a sequence of checks are conducted that govern firing individual lateral pulse jets. The conditions that must be satisfied for an individual lateral pulse jet to fire are as follows:

a. The magnitude of the off-axis trajectory tracking error must be greater than a specified distance.

$$\Gamma > e_{THRES}\,. \tag{17}$$

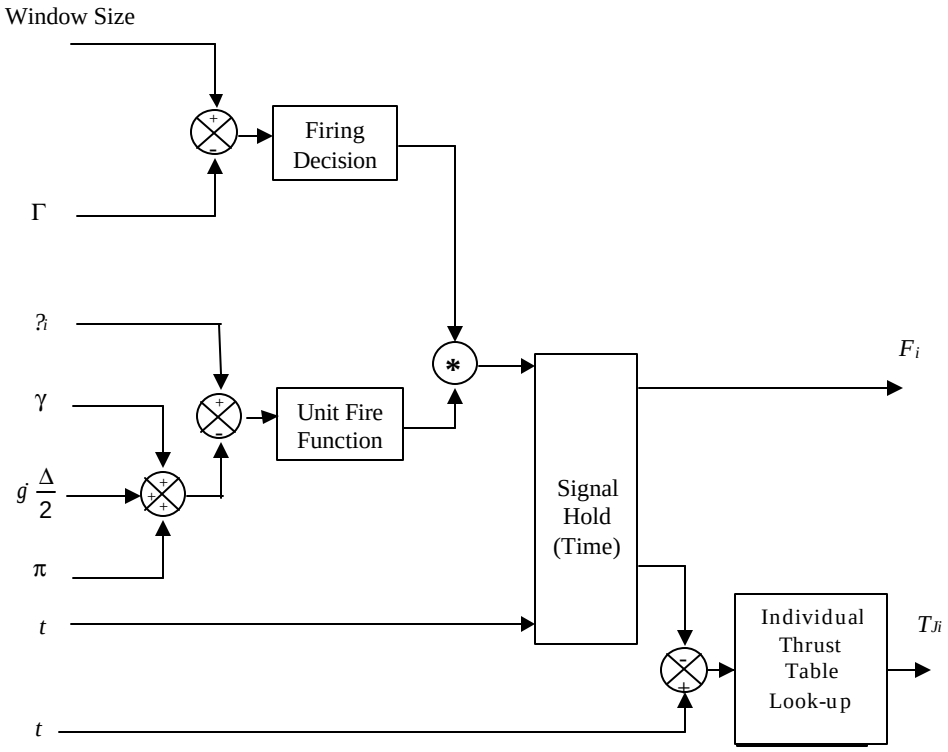

Figure 3. ith individual lateral pulse jet firing logic.

b. The time elapsed since the last lateral pulse jet firing must be greater than a specified duration.

$$t - t^{*} > \Delta t_{THRES} \tag{18}$$

c. The projected angle between the trajectory tracking error and the individual pulse jet force under consideration is less than a specified angle.

$$\left|\theta_i - \pi - \gamma - \dot{\gamma}\Delta_{PJ}\right| Z > \delta_{THRES} \tag{19}$$

d. The individual pulse jet under consideration has not been fired.

The first two checks are valid for all lateral pulse jets, while the last two checks are specific to a given lateral pulse jet. The flight control system contains only three parameters that must be tuned to a specific application, namely, the tracking error window size, the required elapsed time between pulse jet firings, and the angle tolerance between the tracking error and the individual pulse jet force.

4. Results

To investigate the ability of a lateral pulse jet ring to reduce impact point dispersion, the equations of motion described above are numerically integrated using a fourth order Runge-Kutta algorithm. The rocket configuration used in the simulation study to follow is a representative direct-fire rocket that is a 1.4-m-long, fin-stabilized rocket with three popout fins on the rear of the round. The lateral pulse jet ring is located 1.16 m from the base of the rocket. The main rocket motor burns for 1.12 s and imparts an impulse to the rocket of 6,212 N-s. During the main rocket motor burn, the forward velocity of the rocket is increased from 43.7 m/s to 767.5 m/s. The rocket weight, mass center location from the base of the rocket, roll inertia, and pitch inertia before and after burn is 10.4/7.21 kg, 0.85/0.86 m, 0.0077/0.0058 kg m^2, and 1.83/1.61 kg m^2, respectively. Nominally, the rocket exits the launcher with the following initial conditions: x=0.0 m, y=0.0 m, z=-30.5 m, ϕ=0.0 deg, θ=4.14 deg, ψ=0.0 deg, u=43.7 m/s, v=0.0 m/s, w=0.11 m/s, p=51.5 rad/s, q=-0.18 rad/s, and r=0.0 rad/s.

Figures 4–11 compare uncontrolled and controlled trajectories for the example rocket configuration against a nominal command trajectory. The ring contains 32 individual lateral pulse jets, where each individual pulse jet imparts an impulse of 20 N-s on the projectile body over a time duration of 0.01 s. The rocket is launched at an altitude of 30 m toward a target on the ground, and the altitude and cross range equal zero at a range of 3000 m. The trajectory tracking window size is set to 1.5 m, while the pulse jet elapsed time threshold is set to 0.2 s. The pulse jet angle threshold is set to 2°. Figures 4 and 5 plot rocket altitude and cross range vs. range. At the target range of 3000 m, the uncontrolled rocket altitude error is slightly greater than 110 m, while the cross range error is more than 100 m. Compared to the uncontrolled trajectory, the controlled rocket trajectory follows the commanded trajectory well, with an impact error on the order of a couple meters. The off-axis trajectory tracking error, Γ, is plotted in Figure 6. While the uncontrolled rocket trajectory error is greater than 100 m, the trajectory tracking error for the lateral pulse jet controlled rocket remains under 6 m for the entire flight. The sequence of lateral pulse jet firing times is depicted in Figure 12. Twenty two of the possible 32 lateral pulse jets are fired in this particular example. Notice that pulses are fired at a rate that does not exceed 0.2 s. The minimum required time between successive pulses, Δt_{THRES}, is an important design parameter of the flight control system. If Δt_{THRES} is set too low, the rocket does not have sufficient time to respond and many

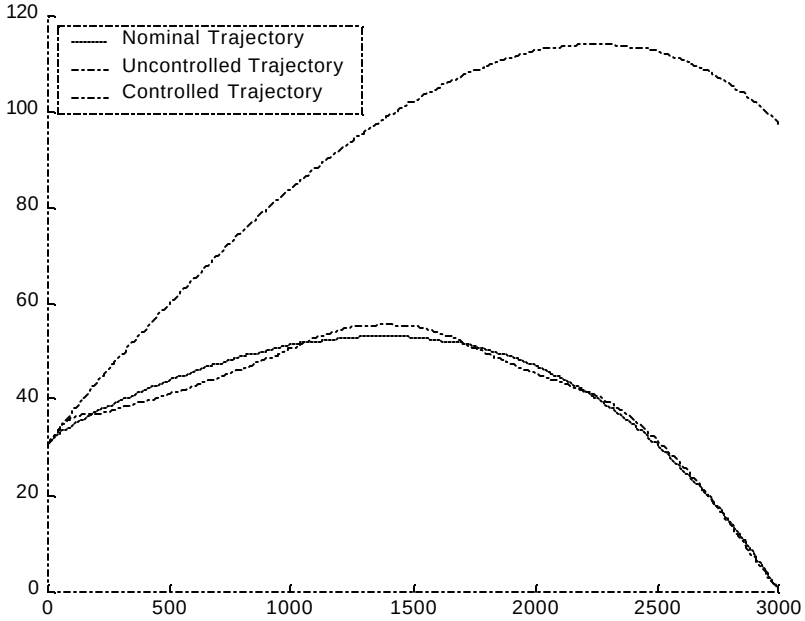

Figure 4. Altitude vs. range.

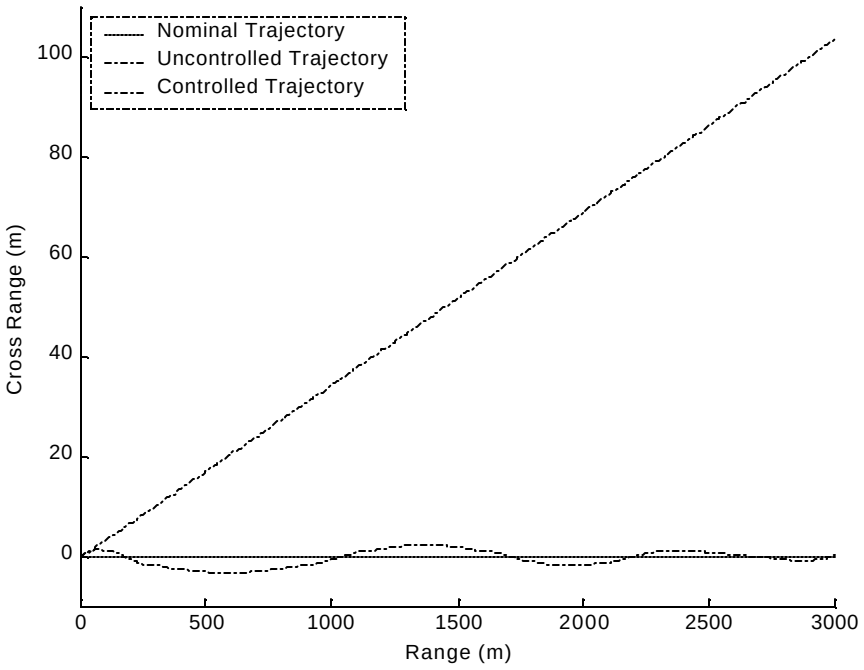

Figure 5. Cross range vs. range.

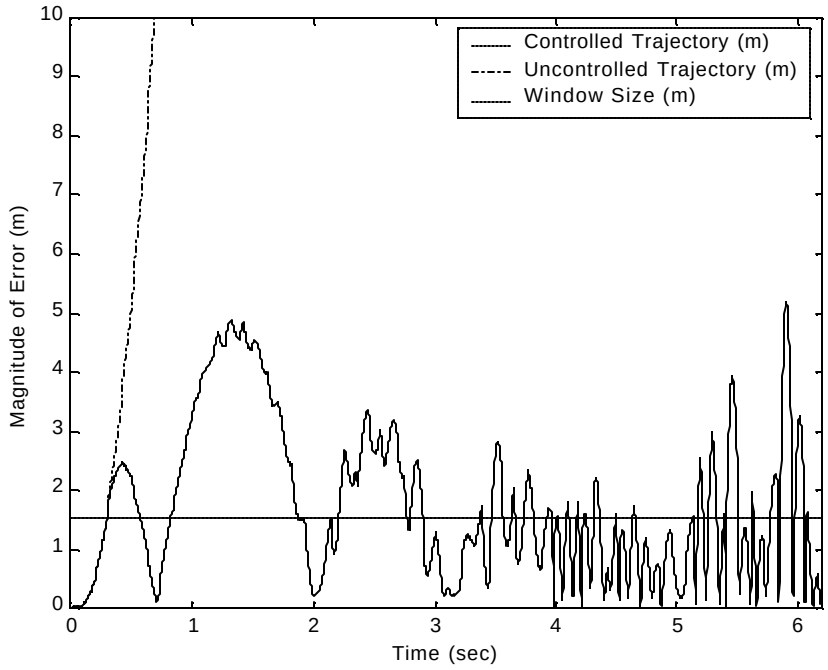

Figure 6. Trajectory tracking error vs. time.

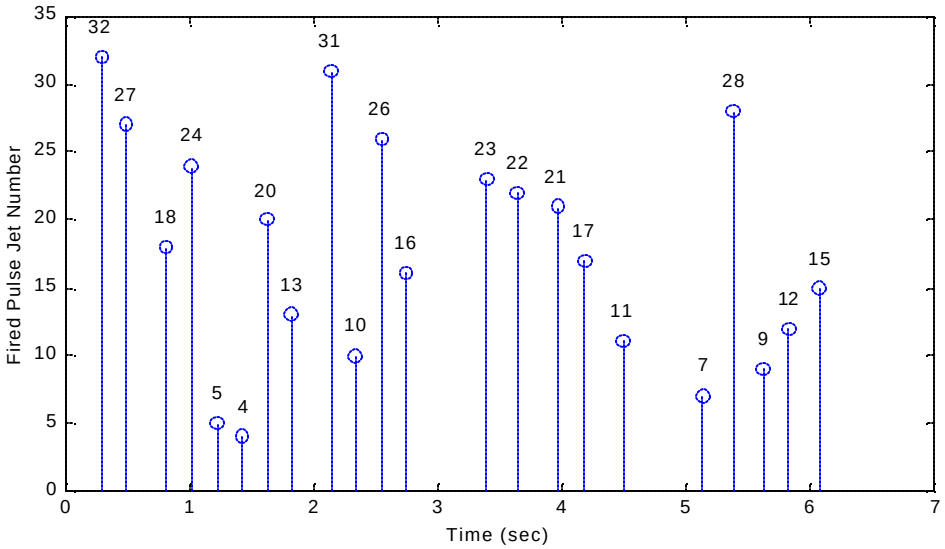

Time.

Figure. 7. Pulse jet firing time.

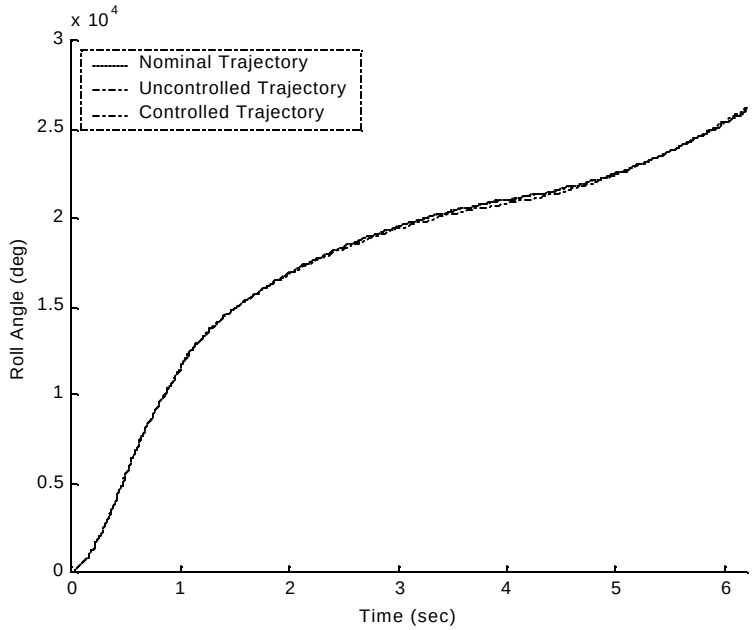

Figure 8. Roll angle vs. time.

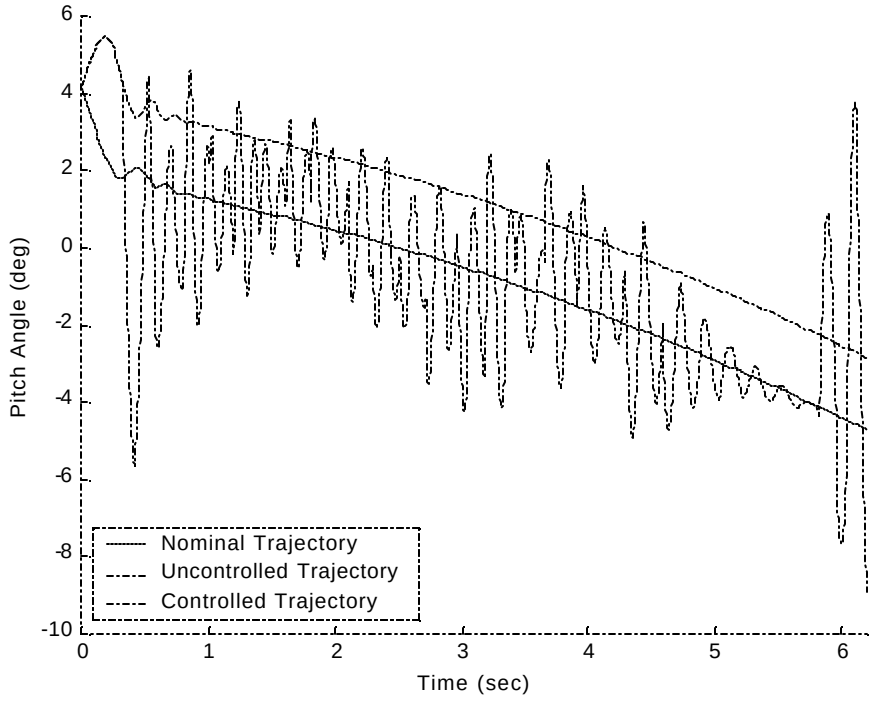

Figure 9. Angle vs. time.

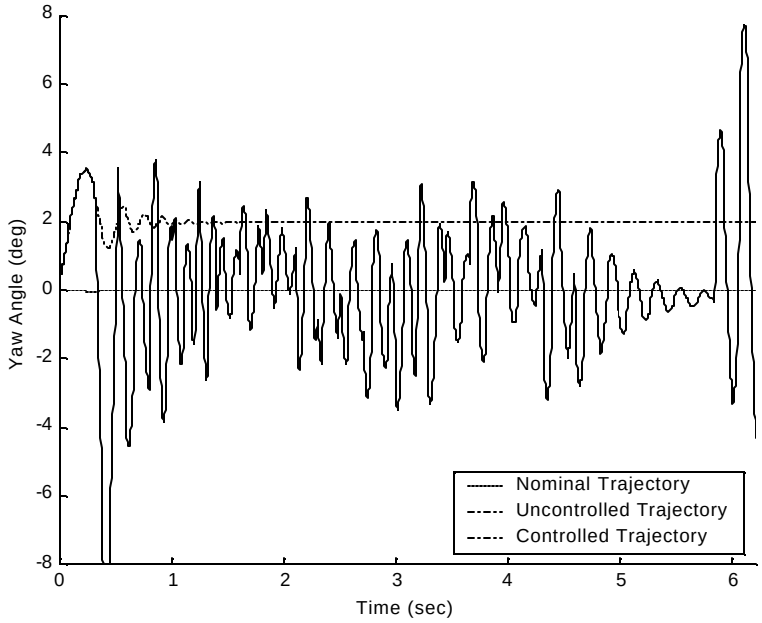

Figure 10. Euler pitch angle vs. time.

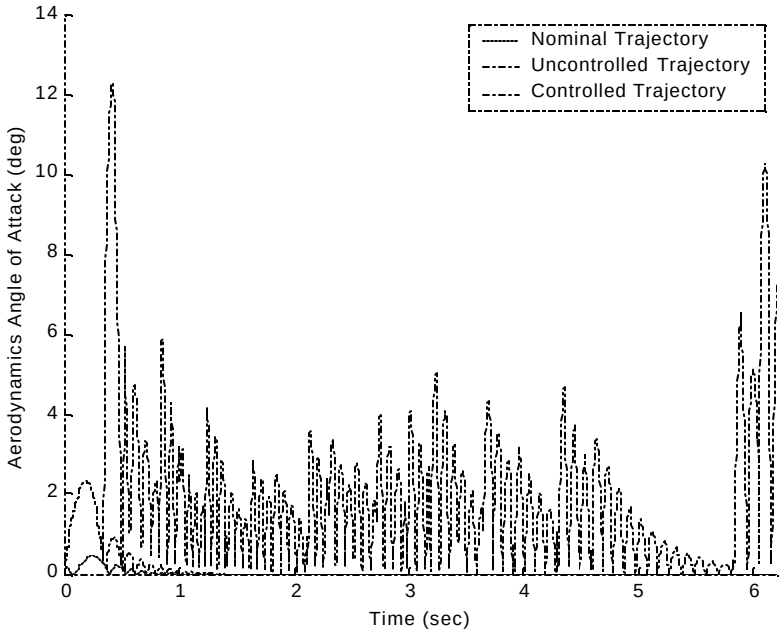

Figure 11. Aerodynamic angle of attack vs. time.

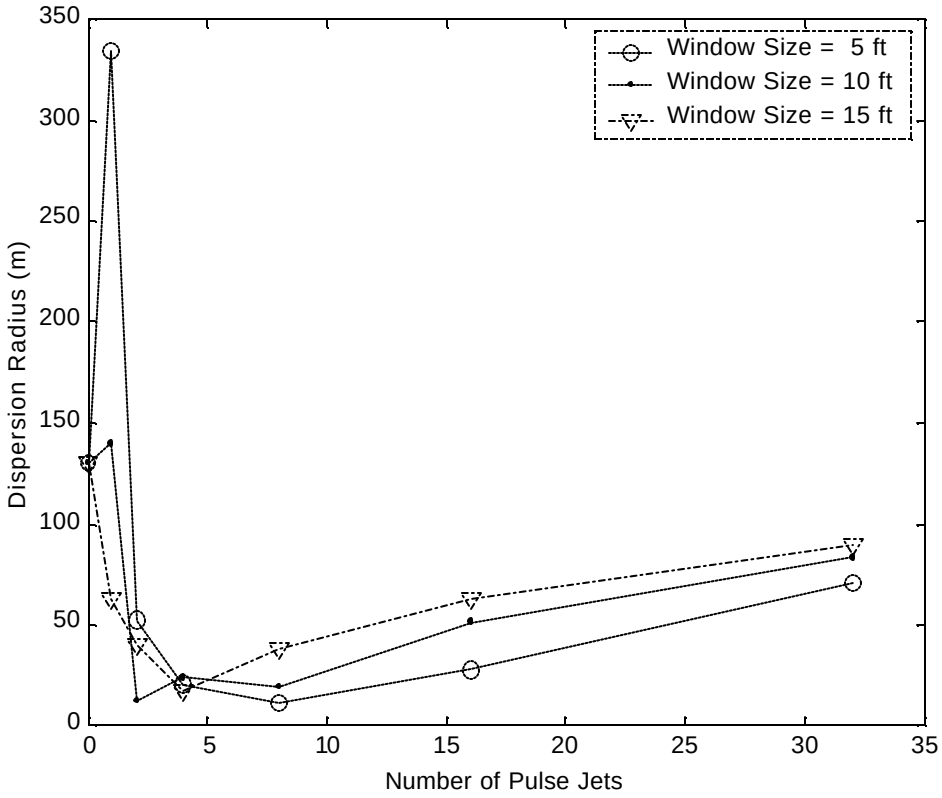

Figure 12. Dispersion radius vs. number of pulse jets and trajectory tracking window size (total ring impulse = 80 N-s,).

pulses will be fired, tending to over compensate for trajectory errors. On the other hand, if Δt_{THRES} is set too high, then only a small number of pulses can possibly be fired and control authority is wasted. In this instance, trajectory tracking will tend to build without pulse jet corrective action.

The roll angle time history is shown in Figure 8; the roll response is essentially unaffected by the action of the lateral pulse jets as both the controlled and uncontrolled roll angle time histories are approximately equal. A comparison of pitch attitude for the uncontrolled and controlled trajectories is provided in Figure 9. While the nominal and uncontrolled trajectories show a steady decrease in pitch attitude as the rocket flies down range, the controlled trajectory shows oscillatory response due to the firing of pulse jets. Total pitch angle excursions of greater than 10° are experienced toward the end of the trajectory. Similar oscillations are seen in the yaw angle time history shown in Figure 10. The aerodynamic angle of attack of the nominal, uncontrolled, and controlled cases are shown in Figure 11. While the angle of attack for the nominal and uncontrolled cases remains relatively small, under 2.5°, the action of pulse jets induces angles of attack greater than 10° near the target.

The initial state of the rocket as it exits the launcher and enters free flight can be viewed as a random process. The random nature of the initial free flight state stems from many effects, but perhaps most notably from launcher and rocket manufacturing tolerances combined with resulting launcher and rocket vibration. Random perturbations in initial free flight conditions create target dispersion impact points. Furthermore, for direct-fire rockets, perturbations in initial off-axis angular rates have been found to significantly contribute to the impact point error budget [7, 8]. Figure 13 compares impact points at a range of 3,000 m for the uncontrolled and controlled direct-fire rocket configurations with a sample size of 50, where the initial pitch rate and yaw rate are independent Gaussian random variables. The mean value for pitch and yaw rate is –0.18 rad / s and 0 rad / s, respectively. The standard deviation for both pitch and yaw rate is 0.3 rad / s. The dispersion radius is defined as the radius of a circle that emanates from the mean impact point and contains 67% of the impact points. The large circle in Figure 12 is the dispersion radius for the uncontrolled case, which is equal to 130.3 m, while the dispersion radius for the controlled case is 1.3 m and is not noticeable on the figure.

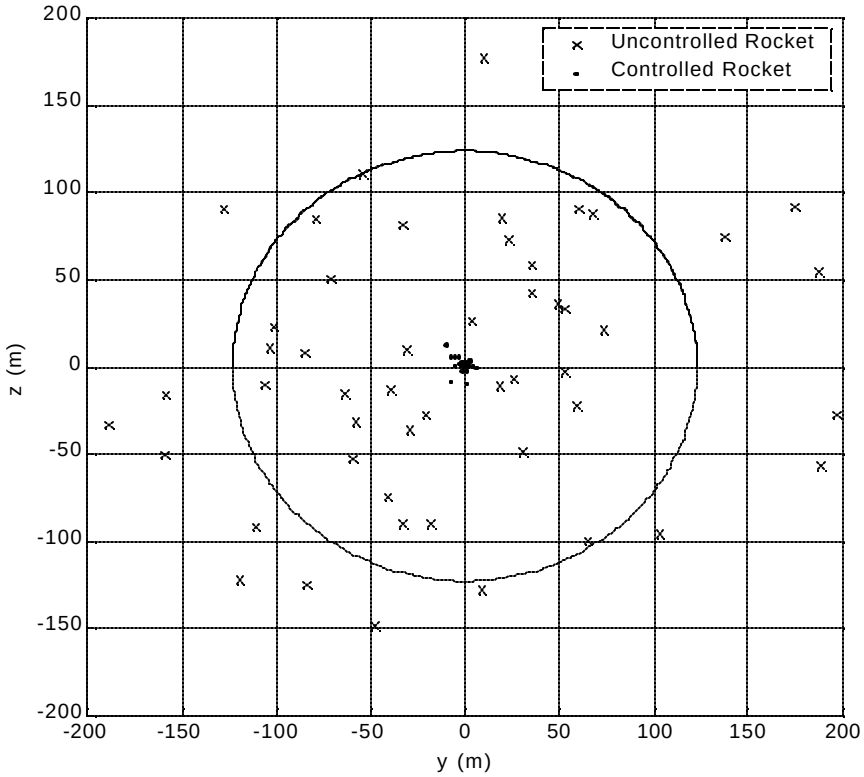

Figure 13. Impact point dispersion (perturbed initial pitch and yaw rate).

Figures 14–16 show the relationship between dispersion radius, number of pulse jets on the ring, and individual pulse jet impulse for three different trajectory tracking window sizes of 1.5 m, 3.0 m, and 4. 5 m. As the number of individual pulse jets is increased, the total impulse contained in the pulse jet ring is increased. In each graph, the trajectory tracking window size is shown as a constant dashed line. When the impulse for the individual lateral pulse jets is small, dispersion radius is steadily reduced as the number of pulse jets or the jet impulse is increased. When the individual lateral pulse jet impulse is relatively large, adding more pulse jets can actually increase the dispersion radius. In this case, the lateral pulse jet impulse is so large compared to the trajectory tracking error, that firing a particular pulse jet tends to over corrects the tracking error. Contrasting Figures 13, 14, and 15 shows that as the trajectory tracking window size is increased, a greater value of jet impulse yields a steady decrease in the dispersion radius as the total number of pulse jets on the ring is increased.

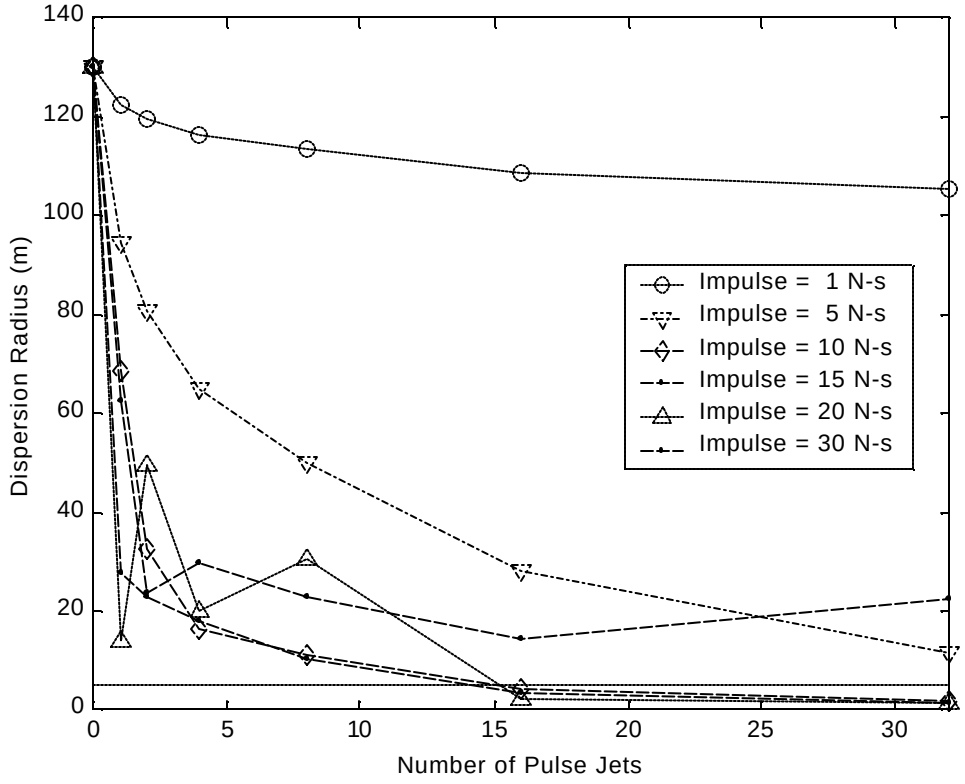

Figure 14. Dispersion radius vs. number of pulse jets and pulse jet impulse (trajectory tracking window size = 1.5 m).

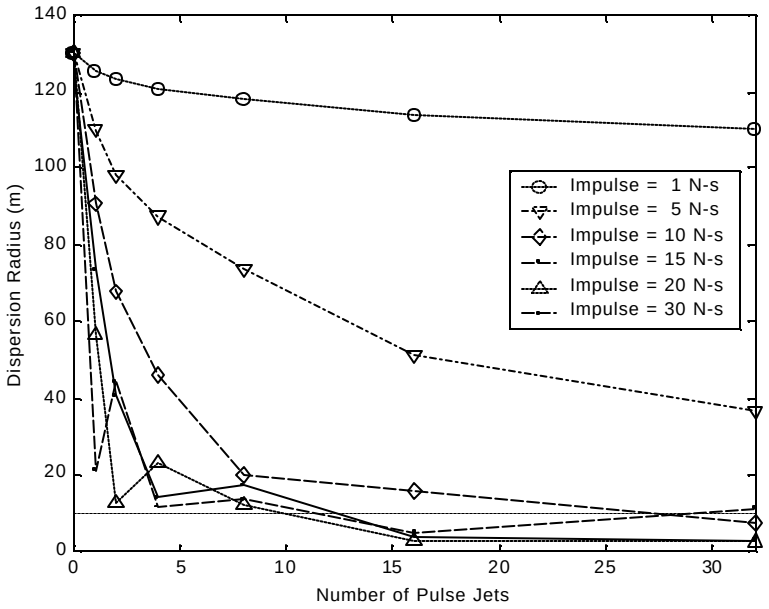

Figure 15. Dispersion radius vs. number of pulse jets and pulse jet impulse (trajectory tracking window size = 3.0 m).

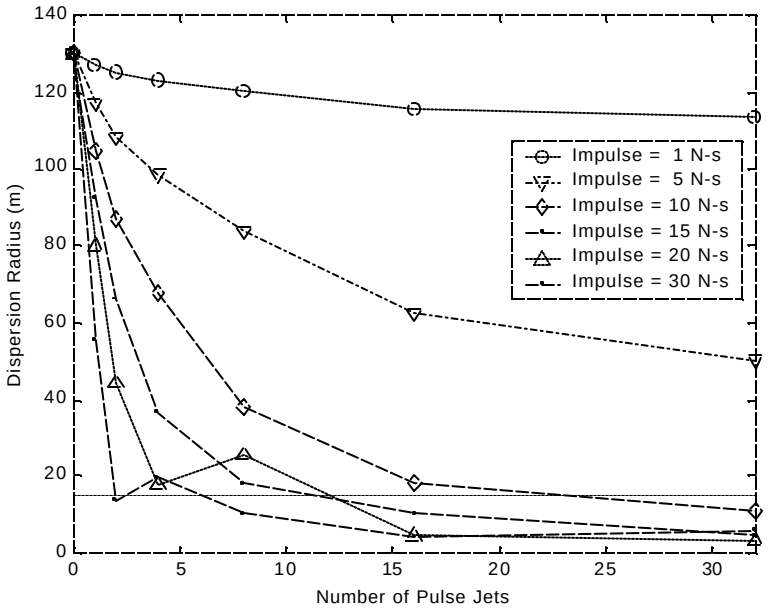

Figure 16. Dispersion radius vs. number of pulse jets and pulse jet impulse (trajectory tracking window size = 4.5 m).

Figure 17 shows the relationship between dispersion radius, number of pulse jets on the ring, and the total ring impulse for a trajectory tracking window size of 1.5 m. Each line on the figure represent lines of constant total ring impulse. For these traces, as the number of lateral pulse jets on the ring is increased, the impulse for an individual lateral pulse jet decreases proportionally so the total ring impulse remains constant. For relatively low total ring impulse, a single lateral pulse jet yields the lowest dispersion radius. The reason for this trend is that the effectiveness of a pulse jet on the trajectory decreases sharply as the projectile flies down range. Hence, a comparatively large and early trajectory correction provides more of an impact point modification than two pulses, each of half impulse strength, where one of the pulses occurs farther down range.

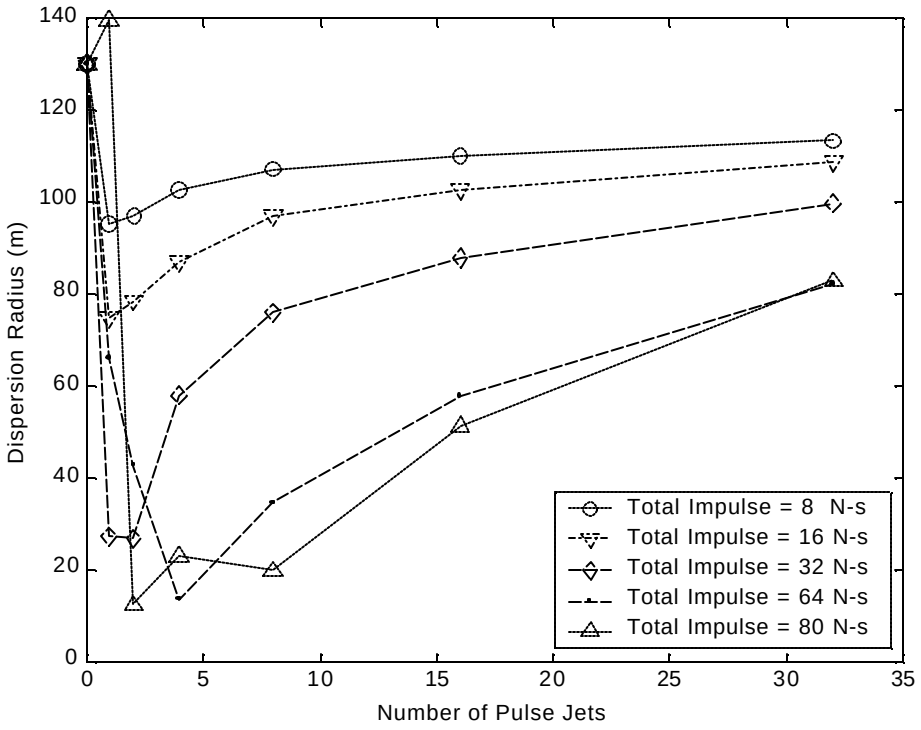

Figure 17. Dispersion radius vs. number of pulse jets and total ring impulse (trajectory tracking window size = 3.0 m).

As the total impulse on the ring is increased, the minimum dispersion radius is decreased. For relatively large total ring impulse, an optimum number of individual lateral pulse jets exists for a given trajectory tracking window size. In the example shown in Figure 16, a total ring impulse of 64 N-s split into four individual lateral pulse jets provides the optimum dispersion reduction. Figure 12 plots the dispersion radius vs. the number of pulse jets for three

different trajectory tracking window sizes. The total ring impulse for all data on the chart is 80 N-s. A single impulse increases the dispersion radius for trajectory tracking window sizes of 1.5 m and 3.0 m. This figure underlines the importance of properly selecting the number of pulse jets and the pulse jet impulse for a particular accuracy design requirement.

Figures 18 and 19 plot dispersion radius as a function of the atmospheric wind angle for the uncontrolled and controlled rocket configurations, respectively. An atmospheric wind angle of 0° corresponds to a direct head wind, whereas an angle of 180° represents a direct tail wind. The uncontrolled rocket configuration is insensitive to direct head and tail winds; in these cases, the rocket range is predominantly effected. On the other hand, side winds induce dispersion over 130 m. The controlled rocket configuration successfully suppresses dispersion to under 6 m for all wind directions.

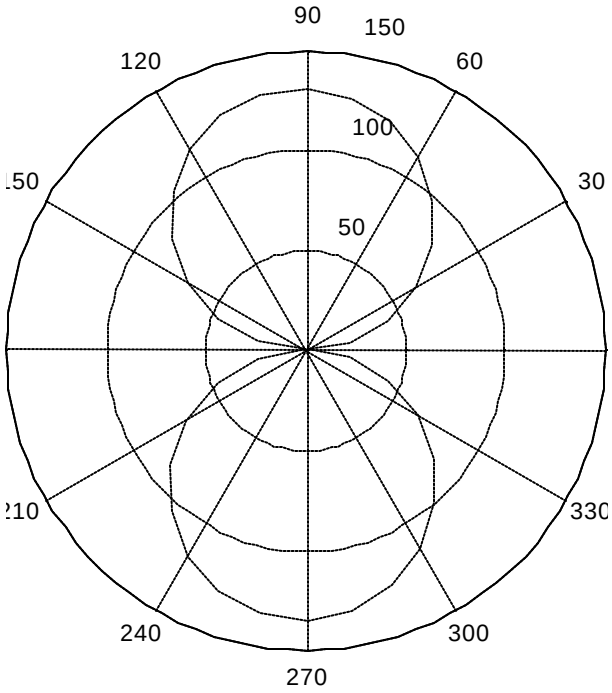

Figure 18. Dispersion radius vs. atmospheric wind direction for the uncontrolled rocket (atmospheric wind speed = 7.6 m/s, number of pulse jets = 32, pulse jet impulse = 20 N-s, trajectory tracking window size = 1.5 m).

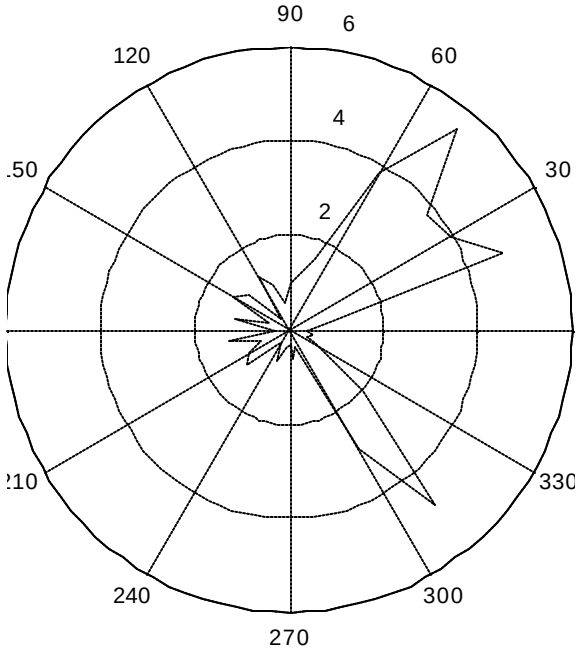

Figure 19. Dispersion radius vs. atmospheric wind direction for the controlled rocket (atmospheric wind speed = 7.6 m/s, number of pulse jets = 32, pulse jet impulse = 20 N-s, trajectory tracking window size = 1.5 m).

5. Conclusions

Using a previously validated six degree of freedom dynamic model of a direct-fire rocket, a drastic reduction in impact point dispersion using a lateral pulse jet control mechanism coupled to a trajectory tracking flight control system is demonstrated. The ability to improve dispersion performance must be weighed against the cost of installing an IMU sensor suite and a pulse jet ring onboard existing unguided direct fire-rockets. In designing a lateral pulse jet control system, the number of pulse jets and the pulse jet impulse must be carefully tuned against the desired impact point dispersion and the level of uncertainty within the rocket.

INTENTIONALLY LEFT BLANK.

6. References

1. Srivastava, B. "Lateral Jet Control of a Supersonic Missile: Computational and Experimental Comparisons." *Journal of Spacecraft and Rockets*, vol. 35, no. 2, pp. 141–146, 1998.

2. Srivastava, B. "Asymmetric Divert Jet Performance of a Supersonic Missile: Computational and Experimental Comparisons." *Journal of Spacecraft and Rockets*, vol. 36, no. 5, pp. 621–632, 1999.

3. Brandeis, J., and J. Gill. "Experimental Investigation of Super- and Hypersonic Jet Interaction on Missile Configurations." *Journal of Spacecraft and Rockets*, vol. 35, no. 3, pp. 296–302, 1998.

4. Harkins, T. E., and T. G. Brown. "Using Active Damping as a Precision-Enhancing Technology for 2.75-Inch Rockets." ARL-TR-1772, U.S. Army Research Laboratory, Aberdeen Proving Ground, MD, 1999.

5. Gast, R., S. Morris, and M. Costello. "Simulation of Shot Impacts for the M1A1 Tank Gun." *Journal of Guidance, Control, and Dynamics*, vol. 23, no. 1, pp. 53–59, 2000.

6. Costello, M., and D. Anderson. "Effect of Internal Mass Unbalance on the Terminal Accuracy and Stability of a Projectile." Proceedings of the 1996 AIAA Flight Mechanics Conference, San Diego, CA, 1996.

7. Carter, R., W. Chase, and J. Whiteside. "Accuracy Analysis for the Advanced Rocket System." FTB-IR-14, U.S. Army Research, Development, and Engineering Center, Picatinny Arsenal, New Jersey, 1994.

8. Bellamy, R., W. Chase, and J. Whiteside. "Accuracy Analysis for the 2.75-inch MK66 Rocket." FTB-IR-23, U.S. Army Research, Development, and Engineering Center, Picatinny Arsenal, New Jersey, 1995.

INTENTIONALLY LEFT BLANK.

List of Symbols

x, y, z - Components of the position vector of center of mass of the composite body in an inertial reference frame.

ϕ, θ, ψ - Euler roll, pitch and yaw angles of the projectile.

u, v, w - Components of the velocity vector of the mass center of the composite body in the body reference frame.

p, q, r - Components of the angular velocity vector of the projectile in the body reference frame.

X, Y, Z - Total applied force components in the aft body reference frame.

L, M, N - Total applied moments about rocket mass center expressed in the aft body reference frame.

u_A, v_A, w_A - Components of the velocity of the mass center of the projectile with mean wind expressed in the body reference frame.

V_A - Magnitude of the velocity vector of the mass center of the projectile experienced with mean wind expressed in the body reference frame.

V_{MW}, σ_{MW} - Magnitude and wind factor of the mean atmospheric wind expressed in the initial reference frame.

ρ - Air density.

D - Rocket reference diameter.

T_{R_i} - i^{th} main rocket motor thrust.

T_{J_i} - i^{th} lateral pulse jet thrust.

$N_{RXi}, N_{RYi}, N_{RZi}$ - i^{th} main rocket motor direction cosines in the body frame.

N_J - Number of individual lateral pulse jets.

e_{THRES} - Trajectory tracking window size.

Δt_{THRES} - Minimum required elapsed time between successive pulse jet firing.

δ_{THRES} - Pulse jet angle threshold.

t^* - Time of the most recent pulse jet firing.

$?_i$ - Angle between $\vec{J}_B$ and the i^{th} pulse jet.

Δ - Pulse jet firing duration.

T - $\dot{\gamma}$ time constant.

C_{X0} - Zero yaw axial force aerodynamic coefficient.

C_{X2} - Yaw axial force aerodynamic coefficient.

C_{NA} - Normal force aerodynamic coefficient.

C_{DD} - Fin cant roll moment aerodynamic coefficient.

C_{LP} - Roll damping aerodynamic coefficient.

C_{MQ} - Pitch damping aerodynamic coefficient.

NO. OF COPIES	ORGANIZATION
2	DEFENSE TECHNICAL INFORMATION CENTER DTIC OCA 8725 JOHN J KINGMAN RD STE 0944 FT BELVOIR VA 22060-6218
1	COMMANDING GENERAL US ARMY MATERIEL CMD AMCRDA TF 5001 EISENHOWER AVE ALEXANDRIA VA 22333-0001
1	INST FOR ADVNCD TCHNLGY THE UNIV OF TEXAS AT AUSTIN 3925 W BRAKER LN STE 400 AUSTIN TX 78759-5316
1	US MILITARY ACADEMY MATH SCI CTR EXCELLENCE MADN MATH THAYER HALL WEST POINT NY 10996-1786
1	DIRECTOR US ARMY RESEARCH LAB AMSRL D DR D SMITH 2800 POWDER MILL RD ADELPHI MD 20783-1197
1	DIRECTOR US ARMY RESEARCH LAB AMSRL CS IS R 2800 POWDER MILL RD ADELPHI MD 20783-1197
3	DIRECTOR US ARMY RESEARCH LAB AMSRL CI OK TL 2800 POWDER MILL RD ADELPHI MD 20783-1197
3	DIRECTOR US ARMY RESEARCH LAB AMSRL CS IS T 2800 POWDER MILL RD ADELPHI MD 20783-1197

NO. OF COPIES	ORGANIZATION
	ABERDEEN PROVING GROUND
2	DIR USARL AMSRL CI LP (BLDG 305)

NO. OF COPIES	ORGANIZATION
3	AIR FORCE RSRCH LAB MUNITIONS DIR AFRL/MNAV G ABATE 101 W EGLIN BLVD STE 219 EGLIN AFB FL 32542
1	CDR WL/MNMF D MABRY 101 W EGLIN BLVD STE 219 EGLIN AFB FL 32542-6810
20	OREGON STATE UNIVERSITY DEPT OF MECHL ENGRG M COSTELLO CORVALLIS OR 97331
4	CDR US ARMY ARDEC AMSTA AR CCH J DELORENZO S MUSALI R SAYER P DONADIO PICATINNY ARESENAL NJ 07806-5000
7	CDR US ARMY TANK MAIN ARMAMENT SYSTEM AMCPM TMA D GUZIEWICZ R DARCEY C KIMKER R JOINSON E KOPOAC T LOUZIERIO C LEVECHIA PICATINNY ARESENAL NJ 07806-5000
1	CDR USA YUMA PROV GRND STEYT MTW YUMA AZ 85365-9103
1	DIR BENET LABORATORIES SMCWV QAR T MCCLOSKEY WATERVLIET NY 12189-5000

NO. OF COPIES	ORGANIZATION
10	CDR US ARMY TACOM AMCPEO HFM AMCPEO HFM F AMCPEO HFM C AMCPM ABMS AMCPM BLOCKIII AMSTA CF AMSTA Z AMSTA ZD AMCPM ABMS S W DR PATTISON A HAVERILLA WARREN MI 48397-5000
1	CDR USAOTEA CSTE CCA DR RUSSELL ALEXANDRIA VA 22302-1458
2	DIR US ARMY ARMOR CTR & SCHL ATSB WP ORSA A POMEY ATSB CDC FT KNOX KY 40121
1	CDR US ARMY AMCCOM AMSMC ASR A MR CRAWFORD ROCK ISLAND IL 61299-6000
2	PROGRAM MANAGER GROUND WEAPONS MCRDAC LTC VARELA CBGT QUANTICO VA 22134-5000
4	COMMANDER US ARMY TRADOC ATCD T ATCD TT ATTE ZC ATTG Y FT MONROE VA 23651-5000

NO. OF COPIES	ORGANIZATION
1	NAWC F PICKETT CODE C2774 CLPL BLDG 1031 CHINA LAKE CA 93555
1	NAVAL ORDNANCE STATION ADVNCD SYS TCHNLGY BRNCH D HOLMES CODE 2011 LOUISVILLE KY 40214-5001
1	NAVAL SURFACE WARFARE CTR F G MOORE DAHLGREN DIVISION CODE G04 DAHLGREN VA 22448-5000
1	US MILITARY ACADEMY MATH SCI CTR OF EXCELLENCE DEPT OF MATHEMATICAL SCI MDN A MAJ DON ENGEN THAYER HALL WEST POINT NY 10996-1786
3	DIR SNL A HODAPP W OBERKAMPF F BLOTTNER DIVISION 1631 ALBUQUERQUE NM 87185
3	ALLIANT TECH SYSTEMS C CANDLAND R BURETTA R BECKER 7225 NORTHLAND DR BROOKLYN PARK MN 55428
3	DIR USARL AMSRL SE RM H WALLACE AMSRL SS SM J EIKE A LADAS 2800 POWDER MILL RD ADELPHI MD 20783-1145

NO. OF COPIES	ORGANIZATION
1	OFC OF ASST SECY OF ARMY FOR R&D SARD TR W MORRISON 2115 JEFFERSON DAVIS HWY ARLINGTON VA 22202-3911
2	CDR USARDEC AMSTA FSP A S DEFEO R SICIGNANO PICATINNY ARESENAL NJ 07806-5000
2	CDR USARDEC AMSTA AR CCH A M PALATHINGAL R CARR PICATINNY ARESENAL NJ 07806-5000
5	TACOM ARDEC AMSTA AR FSA K CHIEFA AMSTA AR FS A WARNASCH AMSTA AR FSF W RYBA AMSTA AR FSP S PEARCY J HEDDERICH PICATINNY ARESENAL NJ 07806-5000
5	CDR US ARMY MICOM AMSMI RD P JACOBS P RUFFIN AMSMI RD MG GA C LEWIS AMSMI RD MG NC C ROBERTS AMSMI RD ST GD D DAVIS RSA AL 35898-5247

NO. OF
COPIES ORGANIZATION

3 CDR US ARMY AVN TRP CMD
DIRECTORATE FOR
ENGINEERING
AMSATR ESW
M MAMOUD
M JOHNSON
J OBERMARK
RSA AL 35898-5247

1 DIR US ARMY RTTC
STERT TE F TD
R EPPS
BLDG 7855
REDSTONE ARSENAL AL
38598-8052

2 STRICOM
AMFTI EL
D SCHNEIDER
R COLANGELO
12350 RESEARCH PKWY
ORLANDO FL 32826-3276

1 CDR OFFICE OF NAVAL RES
CODE 333
J GOLDWASSER
800 N QUINCY ST RM 507
ARLINGTON VA 22217-5660

1 CDR US ARMY RES OFFICE
AMXRO RT IP TECH LIB
PO BOX 12211
RESEARCH TRIANGLE PARK NJ
27709-2211

4 CDR US ARMY AVN TRP CMD
AVIATION APPLIED TECH DIR
AMSATR TI
R BARLOW
E BERCHER
T CONDON
B TENNEY
FT EUSTIS VA 23604-5577

3 CDR NAWC
WEAPONS DIV
CODE 543400D
S MEYERS
CODE C2744
T MUNSINGER
CODE C3904
D SCOFIELD
CHINA LAKE CA 93555-6100

1 CDR NSWC
CRANE DIVISION
CODE 4024
J SKOMP
300 HIGHWAY 361
CRANE IN 47522-5000

1 CDR NSWC
DAHLGREN DIV
CODE 40D
J BLANKENSHIP
6703 WEST HWY 98
PANAMA CITY FL 32407-7001

1 CDR NSWC
J FRAYSEE
D HAGEN
17320 DAHLGREN RD
DAHLGREN VA 22448-5000

5 CDR NSWC
INDIAN HEAD DIV
CODE 40D D GARVICK
CODE 4110C L FAN
CODE 4120 V CARLSON
CODE 4140E H LAST
CODE 450D T GRIFFIN
101 STRAUSS AVE
INDIAN HEAD MD 20640-5000

1 CDR NSWC
INDIAN HEAD DIV
LIBRARY CODE 8530
BLDG 299
101 STRAUSS AVE
INDIAN HEAD MD 20640

2 US MILITARY ACADEMY
MATH SCI CTR OF
EXCELLENCE
DEPT OF MATHEMATICAL SCI
MDN A
MAJ D ENGEN
R MARCHAND
THAYER HALL
WEST POINT NY 10996-1786

3 CDR US ARMY YUMA PG
STEYP MT AT A
A HOOPER
STEYP MT EA
YUMA AZ 85365-9110

NO. OF COPIES	ORGANIZATION
6	CDR NSWC INDIAN HEAD DIV CODE 570D J BOKSER CODE 5710 L EAGLES J FERSUSON CODE 57 C PARIS CODE 5710G S KIM CODE 5710E S JAGO 101 STRAUSS AVE ELY BLDG INDIAN HEAD MD 20640-5035
1	BRUCE KIM MICHIGAN STATE UNIVERSITY 2120 ENGINEERING BLDG EAST LANSING MI 48824-1226
2	INDUSTRIAL OPERATION CMD AMFIO PM RO W MCKELVIN MAJ BATEMAN ROCK ISLAND IL 61299-6000
3	PROGRAM EXECUTIVE OFFICER TACTICAL AIRCRAFT PROGRAMS PMA 242 1 MAJ KIRBY R242 PMA 242 33 R KEISER (2 CPS) 1421 JEFFERSON DAVIS HWY ARLINGTON VA 22243-1276
1	CDR NAVAL AIR SYSTEMS CMD CODE AIR 471 A NAKAS 1421 JEFFERSON DAVIS HWY ARLINGTON VA 22243-1276
4	ARROW TECH ASSOCIATES INC R WHYTE A HATHAWAY H STEINHOFF 1233 SHELBOURNE RD SUITE D8 SOUTH BURLINGTON VT 05403

NO. OF COPIES	ORGANIZATION
3	US ARMY AVIATION CTR DIR OF COMBAT DEVELOPMENT ATZQ CDM C B NELSON ATZQ CDC C T HUNDLEY ATZQ CD G HARRISON FORT RUCKER AL 36362
	ABERDEEN PROVING GROUND
3	CDR USA ARDEC AMSTA AR FSF T R LIESKE J WHITESIDE J MATTS BLDG 120
1	CDR USA TECOM AMSTE CT T J SCHNELL RYAN BLDG
3	CDR USA AMSAA AMXSY EV G CASTLEBURY R MIRABELLE AMXSY EF S MCKEY
49	DIR USARL AMSRL WM I MAY T ROSENBERGER AMSRL WM BA W HORST JR W CIEPELLA F BRANDON T BROWN (5 CPS) L BURKE J CONDON B DAVIS T HARKINS (5 CPS) D HEPNER V LEITZKE M HOLLIS A THOMPSON G BROWN

NO. OF
COPIES ORGANIZATION

ABERDEEN PROVING GROUND (CONT)

AMSRL WM BB
B HAUG
AMSRL WM BC
P PLOSTINS (4 CPS)
G COOPER
B GUIDOS
J SAHU
M BUNDY
K SOENCKSEN
D LYON
AMSRL WM BC
J BENDER
J NEWILL
J GARNER
V OSKAY
S WILKERSON
W DRYSDALE
R COATES
A MIKHAL
J WALL
AMSRL WM BD
B FORCH
AMSRL WM BE
M SCHMIDT
AMSRL WM BF
J LACETERA
P HILL
AMSRL WM BR
C SHOEMAKER
J BORNSTEIN

REPORT DOCUMENTATION PAGE

Form Approved
OMB No. 0704-0188

1. AGENCY USE ONLY *(Leave blank)*	2. REPORT DATE	3. REPORT TYPE AND DATES COVERED
	April 2001	Final, October 2000–February 2001

4. TITLE AND SUBTITLE
Dispersion Reduction of a Direct-Fire Rocket Using Lateral Pulse Jets

5. FUNDING NUMBERS
1L162618.H8

6. AUTHOR(S)
Thanat Jitpraphai* and Mark Costello*

7. PERFORMING ORGANIZATION NAME(S) AND ADDRESS(ES)
Oregon State University
Department of Mechanical Engineering
Corvallis, Oregon 97331

8. PERFORMING ORGANIZATION REPORT NUMBER

9. SPONSORING/MONITORING AGENCY NAMES(S) AND ADDRESS(ES)
U.S. Army Research Laboratory
ATTN: AMSRL-WM-BC
Aberdeen Proving Ground, MD 21005-5066

10. SPONSORING/MONITORING AGENCY REPORT NUMBER
ARL-CR- 465

11. SUPPLEMENTARY NOTES

12a. DISTRIBUTION/AVAILABILITY STATEMENT
Approved for public release; distribution is unlimited.

12b. DISTRIBUTION CODE

13. ABSTRACT *(Maximum 200 words)*

The impact point dispersion of a direct-fire rocket can be drastically reduced with a ring of appropriately sized lateral pulse jets coupled to a trajectory tracking flight control system. The system is shown to work well against uncertainty in the form of initial off-axis angular velocity perturbations as well as atmospheric winds. In an example case, dispersion was reduced by a factor of 100. Dispersion reduction is a strong function of the number of individual pulse jets, the pulse jet impulse, and the trajectory tracking window size. Properly selecting these parameters for a particular rocket and launcher combination is required to achieve optimum dispersion reduction. For relatively low pulse jet impulse, dispersion steadily decreases as the number of pulse jets is increased or as the pulse jet impulse is increased. For a fixed total pulse jet ring impulse, a single pulse is the optimum pulse jet configuration when the pulse jet ring impulse is small due to the fact that the effect of a pulse on the trajectory of a rocket decreases as the round flies down range.

14. SUBJECT TERMS	15. NUMBER OF PAGES
guided munition	32
	16. PRICE CODE

17. SECURITY CLASSIFICATION OF REPORT	18. SECURITY CLASSIFICATION OF THIS PAGE	19. SECURITY CLASSIFICATION OF ABSTRACT	20. LIMITATION OF ABSTRACT
UNCLASSIFIED	UNCLASSIFIED	UNCLASSIFIED	UL

INTENTIONALLY LEFT BLANK.